Whalley RD, Choi KS.

The starting vortex in quiescent air induced by dielectric-barrier-discharge plasma.

***Journal of Fluid Mechanics* 2012, 703, 192-203.**

J. Fluid Mech. (2013), *vol.* 703, *pp.* 192–203.

doi:10.1017/jfm.2012.206

The starting vortex in quiescent air induced by dielectric-barrier-discharge plasma

Richard D. Whalley and Kwing-So Choi†

Faculty of Engineering, University of Nottingham, University Park, Nottingham NG7 2RD, UK

(Received 23 February 2012; revised 5 April 2012; accepted 23 April 2012;
first published online 12 June 2012)

The flow field around an asymmetric dielectric-barrier-discharge (DBD) plasma actuator in quiescent air is studied using particle image velocimetry (PIV) and smoke-flow visualization. On initiation of DBD plasma a starting vortex is created, which rolls up to form a coherent structure. The starting vortex becomes self-similar when the maximum velocity induced by the DBD plasma actuator reaches a steady state. Here, the plasma jet momentum increases linearly with time, suggesting that the DBD plasma actuator entrains and accelerates the surrounding fluid with a constant force. The wall-parallel and wall-normal distances of the vortex core are observed to scale with $t^{2/3}$ as it travels at 31° to the wall. The velocity of the starting vortex is found to scale with $t^{-1/3}$, while the circulation induced by the plasma actuator scales with $t^{1/3}$.

Key words: vortex dynamics

1. Introduction

Dielectric-barrier-discharge (DBD) plasma actuators have unique properties. They are completely electrical devices requiring no moving parts, which makes their design simple and without the need for complicated ducting, holes or cavities. They are fast-acting with response times of the order of tens of microseconds and they are low in power consumption needing typically tens of watts per metre. The plasma actuators are very light, being of the order of tens of grams per square metre. They are cheap to manufacture and can be retrofitted to existing airframes. For these reasons the past decade has seen a vast increase in research on non-thermal surface plasmas, with their application to the aerospace industry (Moreau 2007; Corke, Enloe & Wilkinson 2010).

Typical DBD plasma actuators consist of an upper and lower electrode separated by a thin dielectric material, with the upper electrode exposed to the air and the lower electrode encapsulated by the aerodynamic surface: see figure 1. On application of several kilovolts of AC power at kHz frequency between the upper and lower electrodes, the air around the upper electrode becomes ionized and plasma is formed. The plasma generates a body force, which entrains and accelerates the surrounding air to induce a jet flow. The body force is caused by the movement of plasma ions to and from the dielectric surface, which is usually referred to as an ionic wind (Robinson 1962).

† Email address for correspondence: kwing-so.choi@nottingham.ac.uk

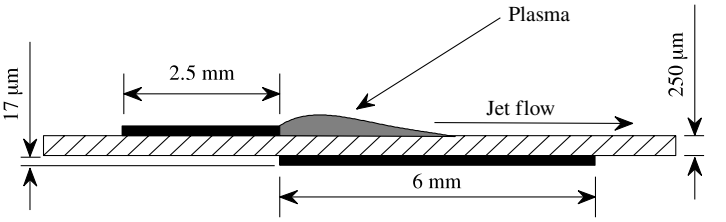

FIGURE 1. Schematic representation of a DBD plasma actuator used in the present study.

On initiation of DBD plasma a starting vortex is created (Whalley & Choi 2010), which convects along and away from the wall with continual plasma forcing and leads to the formation of a laminar wall jet (Jukes *et al.* 2006). However, to date there is little information detailing the development of the starting vortex generated by DBD plasma. Our goals are to provide scaling laws for the development of the starting vortex and establish any self-similar behaviour. These are achieved by studying the flow field near the plasma actuator using particle image velocimetry (PIV) and flow visualization.

The development of a transient wall jet from a thin slit which rolled up into a vortical structure was studied numerically by Conlon & Lichter (1995). They found that the vortical structure convected away from the wall when sufficient secondary vorticity in the inner layer of the wall jet rolled up to create a secondary vortex, which caused the formation of a dipole. They also found that insufficient inner-layer vorticity led to the formation of a monopole, which convected along but with little growth away from the wall. A different vortical behaviour was observed by Allen & Chong (2000) during their experimental investigation of a piston moving through a circular cylinder. When the piston was set into motion, the developing shear layer rolled up to form a piston vortex. They found that secondary vorticity generated continuously at the piston face did not roll up to form a dipole, yet there was apparent growth of the piston vortex along and away from the wall. The resulting trajectory of the piston vortex core was shown to scale with $t^{0.85+m}$, when the speed of the piston was given by the power law with t^m. Here, t is the time.

A recent study of the development of a junction vortex generated as an impulsively started moving belt slid beneath a stationary wall was studied experimentally by Allen & Naitoh (2007). They were able to show that the transient structure had self-similar behaviour over a range of Reynolds numbers with the core of the junction vortex scaling with $t^{5/6}$. Allen & Lopez (2007) performed a numerical simulation of the same junction flow. They found that the flow was dominated by viscosity at the start and the trajectory of the junction vortex core scaled with $t^{1/2}$. As the Reynolds number increased, the junction vortex core scaled with $t^{5/6}$, as found experimentally.

2. Experimental set-up and procedure

The experimental set-up for the PIV and the smoke-flow visualizations is shown in figure 2. The experiments were performed inside a closed chamber to make sure that the flow induced by the DBD plasma actuator was not influenced by any external draughts. The PIV measurements were performed inside a 300 mm × 300 mm square chamber which was 600 mm in length, and the smoke-flow visualizations were performed inside a 508 mm × 508 mm octagonal chamber which was 1.5 m in length. Quantitative measurements of the flow field were obtained with a time-

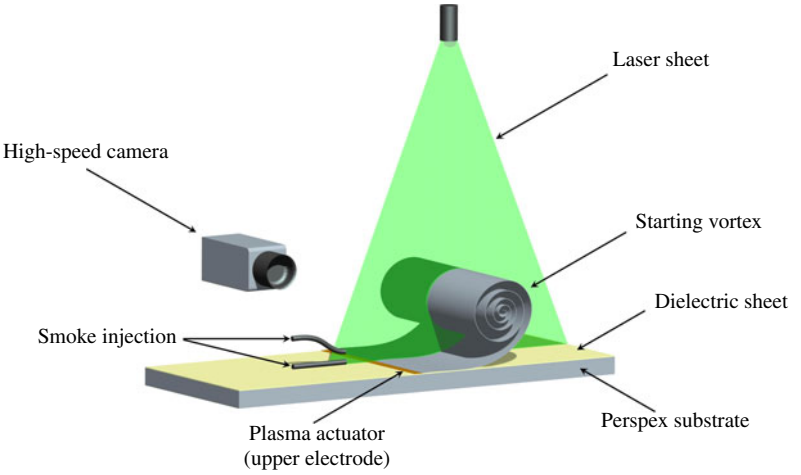

FIGURE 2. (Colour online) Schematic diagram of the experimental set-up for the smoke-flow visualizations and PIV measurements.

Cases	E (kV$_{p-p}$)	f (kHz)	U_0 (m s^{-1})	F_x (mN m^{-1})	C_x
A	5.50	20	0.45	0.16	0.059
B	7.20	20	1.19	1.62	0.211
C	5.50	25	1.36	2.18	0.219

TABLE 1. Experimental conditions studied, velocity scales and plasma force coefficients.

resolved PIV system from TSI. This consisted of a Photron Fastcam APX camera (1024 × 1024 pixels), a New Wave Research Pegasus PIV laser and a TSI 9307-6 oil droplet generator. The camera was set to view an area of 70 mm × 40 mm, and image pairs were taken at a frequency of 500 Hz, with the time delay between frames being typically 200–400 μs. Olive oil with a nominal size of 1 μm was used to seed the air. Data processing was performed with INSIGHT 3G software from TSI, using a cross-correlation algorithm to generate vectors over a 20 × 20 pixel interrogation area with 50 % overlap to an accuracy of 3–5 % (Westerweel 1997). The smoke-flow visualizations were carried out with a Photron Fastcam SA-3 high-speed camera (1024 × 1024 pixels), which was synchronized to a pulsed copper vapour laser. The camera was set to view an area of 60 mm × 30 mm and images were acquired at a frequency of 1 kHz. The air was seeded with water-soluble glycol-based fog from Soundlab using two circular tubes of 5 mm in diameter.

The DBD plasma actuator used in this study was photochemically etched from a copper-clad Mylar sheet (250 μm thick, dielectric constant $\varepsilon = 3.1$: see figure 1) and had 17 μm thick upper and lower electrodes with widths of 2.5 mm and 6 mm, respectively. The total length of the actuator was 160 mm. Similar actuators have been used in flow-separation control of a circular cylinder (Jukes & Choi 2009) and turbulent boundary-layer control for skin-friction drag reduction (Choi, Jukes & Whalley 2011). Here, the plasma was formed by applying sinusoidal AC waveforms with $E = 5.50$–7.20 kV$_{p-p}$ at frequencies $f = 20$–25 kHz. The DBD plasma actuator was operated for durations $t = 150$, 300 and 600 ms with 100 % duty cycle. A summary of the test conditions, denoted by cases A–C, can be found in table 1.

Both the PIV measurements and the smoke-flow visualizations were used to measure the trajectory of the vortex core. The non-dimensional distance that the vortex core has travelled in the horizontal direction (x-direction) from the end of the upper electrode is x_c^* ($=x_c U_0/\nu$, where U_0 is a velocity scale of the vortex to be determined later and ν is the kinematic viscosity) and the distance that the vortex core has travelled normal to the wall (y-direction) is y_c^* ($=y_c U_0/\nu$). Using PIV, three separate experiments were performed for cases A–C (see table 1) under the same conditions. The data obtained over the three experimental runs were phase-averaged every $t = 2$ ms ($t^* = tU_0^2/\nu = 25$–250) with the vortex core being located using a minimum velocity criterion with an accuracy of ± 0.35 mm ($x_c^* = y_c^* = \pm 10$–30). The location of the vortex core using smoke-flow visualizations was identified by observing the swirl of smoke around a point on the high-speed camera picture. The vortex core locations were phase-averaged every $t = 5$ ms ($t^* = 60$–625) over 20–25 events, whose uncertainty in the x_c and y_c measurements was ± 1–2 mm ($x_c^* = \pm 30$–180) and ± 0.8 mm ($y_c^* = \pm 25$–70), respectively.

The body force generated by a DBD plasma actuator is inherently small, being typically of the order of 1–10 mN m^{-1} depending on the voltage and frequency supplied to the plasma actuator (Kriegseis, Grundmann & Tropea 2011), which makes direct force measurements difficult. Therefore, in this study, the momentum of flow induced by DBD plasma in the x-direction, M_x, was obtained from the time-resolved PIV velocity fields by integrating the U-component velocity over each PIV image (Jukes & Choi 2009). This allows the body force to be calculated by computing the rate of change of momentum per unit width (z-direction), $F_x = \mathrm{d}M_x/\mathrm{d}t$, where $M_x = \rho \int_A U \, \mathrm{d}A$. Here, A is the total area of each PIV image from $x = -10$–60 mm and $y = 0$–40 mm. The body force obtained is the total force generated by the plasma actuator minus the shear force acting on the wall due to skin friction. Here, the skin-friction force was estimated using the empirical friction law of a flat plate in a laminar flow, to give approximately 10 % of the total plasma-induced force. Non-dimensional body force is given by the force coefficient, $C_x = 2F_x/\rho U_0^2 L$, where F_x is the body force generated by the plasma actuator in the x-direction, ρ is the fluid density, U_0 is the maximum induced velocity and L is the distance in the x-direction that the vortex core has travelled before the steady-state condition is reached: see table 1.

Further details of experimental set-up and procedure can be found in Whalley (2011), which also includes a complete set of results and discussions on all cases being investigated.

3. Results and discussions

3.1. *Development of the starting vortex*

Figure 3 shows a series of images of the starting vortex on initiation of DBD plasma with an applied voltage $E = 5.50$ kV$_{p\text{–}p}$ at frequency $f = 20$ kHz (case A). The plasma actuator was operated continuously for a duration of $t = 300$ ms ($t^* = 4050$). The smoke-flow visualizations (a–c) and PIV vorticity data (d–f) in figure 3 were taken in the same experimental test conditions, but they were obtained separately. The white dots in the flow visualization data and vorticity data indicate the location of the vortex core. The plasma initiates at $(x^*, y^*) = 0$ and extends for approximately 2–3 mm ($x^* = 60$–90) in the positive x-direction (to the right in figure 1). The starting vortex, through figures 3(a)–3(c), rolls up to form a coherent structure. With time, the starting vortex moves along in the positive x- and y-directions (away from the wall). As the

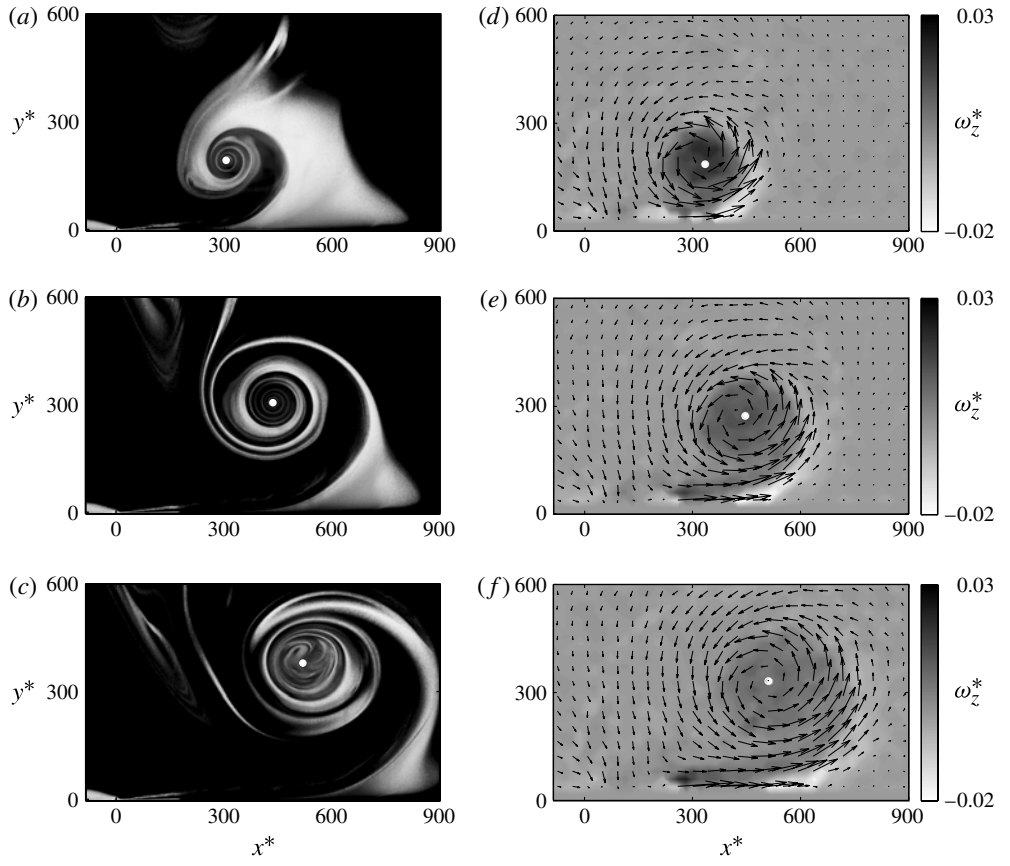

FIGURE 3. (*a–c*) Smoke-flow visualizations showing (*a*) $t^* = 1620$, (*b*) $t^* = 2700$, and (*c*) $t^* = 3780$. (*d–f*) PIV vorticity fields showing (*d*) $t^* = 1620$, (*e*) $t^* = 2700$, and (*f*) $t^* = 3780$ of the starting vortex generated for case A with plasma duration $t^* = 4050$ ($t = 300$ ms). The white dots indicate the centre of the vortex core in the flow visualization and PIV data.

vortex rolls up, the number of turns is increased and a tightly compacted spiral of white smoke is formed.

The non-dimensional vorticity, $\omega_z^*(=\omega_z \nu/U_0^2)$, of a starting vortex is shown in figure 3(*d–f*). In each image the vortex core is located in the region of primary vorticity and coincides with the circling $U-$ and $V-$ component velocity arrows. A region of secondary vorticity can be seen along the wall underneath the primary vorticity region. The secondary vorticity is being stretched and wrapped around the starting vortex. The vorticity distributions show no evidence of dipole formation, at least for the voltage and frequencies of the DBD plasma actuator investigated here. As time increases through figures 3(*d*)–3(*f*), the magnitude of both primary and secondary vorticity decreases as the vortex increases in size and moves along and away from the wall. The location of the vortex core identified by the PIV technique is very similar to that by smoke-flow visualization. However, the vortex core locations in the PIV data are slightly closer to the wall by approximately $y = \pm 0.8$ mm or $y^* = \pm 30$ as compared to flow visualization, which is well within the uncertainty of the measurement techniques.

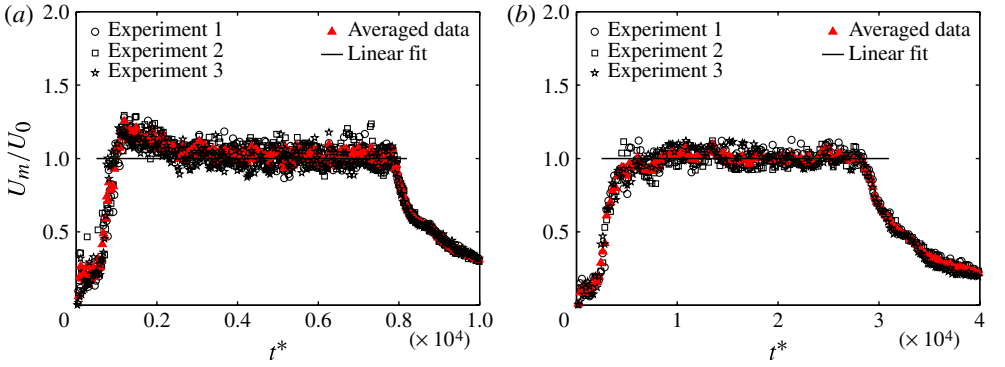

FIGURE 4. (Colour online) The change in maximum velocity induced by the DBD plasma actuator, which is non-dimensionalized by the steady-state value, U_0, for (*a*) case A with plasma duration $t^* = 8100$ ($t = 600$ ms) and (*b*) case B with plasma duration $t^* = 28100$ ($t = 300$ ms).

Figure 4(*a*) shows the maximum velocity, U_m, induced by the plasma actuator for case A with a duration of $t = 600$ ms ($t^* = 8100$), which was located in the wall jet underneath the vortex core. The data shown in figure 4(*a*) have been acquired over 3 separate runs and show that the maximum velocity increases from zero, overshoots and then becomes constant at approximately $t^* = 3000$. This steady-state velocity defines the velocity scale, U_0 of the starting vortex from the plasma actuator. Plasma actuation is stopped at $t = 600$ ms ($t^* = 8100$) when the maximum velocity begins to return to zero. Similar behaviour has been observed when DBD plasma was actuated in quiescent air over a circular cylinder (Jukes & Choi 2009), where the maximum velocity reached a steady state only after a small overshoot. The velocity scale, U_0, for the DBD plasma actuator operated with the parameters for case B with duration $t = 300$ ms ($t^* = 28\,300$) can be found in figure 4(*b*). An overshoot in maximum velocity was not observed in this case, nor for case C (not shown). Instead, the maximum velocity increases from zero and becomes constant at approximately $t^* = 6000$. Gherardi *et al.* (2000) and Shin & Raja (2007) observed that the peak current density of the plasma actuator had a transient response, exhibiting an initial overshoot before reaching a steady state. They also found that the time required to reach a steady state was increased with a reduction in applied voltage to the plasma actuator. It is, therefore, conjectured that the current density of the plasma actuator has not reached a steady state for case A. The velocity scale, U_0, for each case can be found in table 1. The smallest velocity scale with $U_0 = 0.45$ m s^{-1} is found in case A when the smallest voltage and frequency were applied. As the plasma parameters are changed by an increase in voltage (case B) or in frequency (case C), the velocity scale increases to $U_0 = 1.19$ m s^{-1} and $U_0 = 1.36$ m s^{-1}, respectively.

The body force created by DBD is not constant throughout an AC cycle, as shown by Enloe, McHarg & McLaughlin (2008). However, the high frequency of operation of the order of several kHz and hydrodynamic inertia of the induced flow (Kotsonis, Ghaemi & Scarano 2011) resulted in a quasi-steady force in other measurements (Kriegseis *et al.* 2011). The temporal evolution of momentum, M_x, for case A with duration $t = 600$ ms ($t^* = 8100$) can be seen in figure 5(*a*). The momentum seems to increase linearly with time once the vortex has reached a steady state for $t^* > 3000$, so a straight line can be fitted through the data. This suggests that the DBD plasma

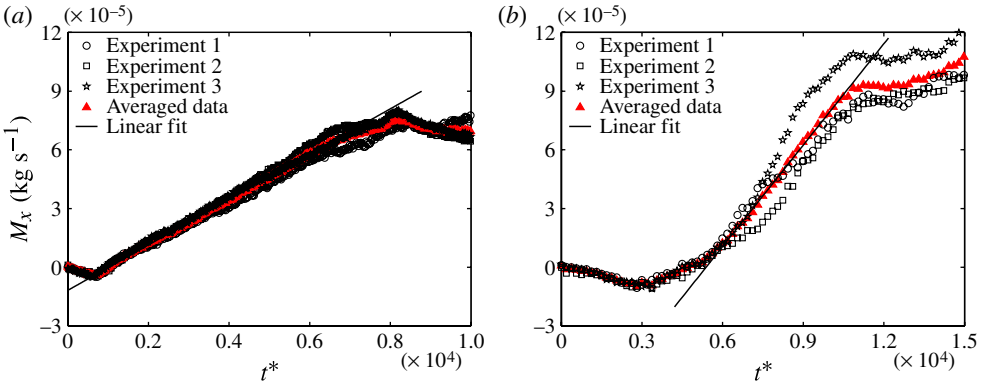

FIGURE 5. (Colour online) Momentum induced by the DBD plasma actuator for (*a*) case A with plasma duration $t^* = 8100$ ($t = 600$ ms) and (*b*) case B with plasma duration $t^* = 28\,100$ ($t = 300$ ms).

actuator has created a constant force, which is in agreement with the recent results of Kriegseis *et al.* (2011). The plasma actuation is stopped at $t^* = 8100$ where the momentum begins to decrease. There is some negative momentum shown in the figure for $t^* < 1000$, since the velocity close to the wall was difficult to measure using PIV due to the glare from the shiny Mylar surface. The momentum induced by the DBD plasma actuator for case B with duration $t = 300$ ms is presented in figure 5(*b*). In this case, some of the plasma-induced flow moved out of the PIV measurement area, which gives an error in the measured momentum for $t^* > 11\,000$. However, the linear region of early momentum growth for case B can also be seen in figure 5(*b*). The rate of change in momentum gives the force per unit width generated by the plasma actuator (see table 1), confirming that the forces are of the order of 1 mN m^{-1} for all cases studied (Enloe *et al.* 2004). The lowest plasma force is generated by the lowest applied voltage and frequency (case A). As the voltage or frequency is increased, the plasma force increases accordingly.

The observations of the formation and development of the starting vortex which have been described are presented schematically in figure 6. As the upper electrode of the DBD plasma reaches the breakdown voltage, plasma ions are transferred to and from the dielectric surface and couple momentum to the fluid in the horizontal direction along the wall: see figure 6(*a*). To replenish the fluid that has been ejected laterally, entrainment occurs directly above the plasma region to form a starting vortex: see figure 6(*b*). Here, the velocity gradient $\partial V/\partial x$ due to the vertical entrainment of fluid and $\partial U/\partial y$ due to the horizontal flow by the plasma force contribute to the generation of vorticity and hence to the circulation of the starting vortex. To preserve the no-slip boundary condition, secondary vorticity is generated at the wall, as illustrated in figure 6(*c*). The starting vortex is then wrapped around by the secondary vorticity, which steers the trajectory away from the wall.

3.2. *Self-similarity of the starting vortex*

The temporal development of the vortex core for cases A–C is presented in figure 7, where 14 data sets are shown in each plot, 7 from the PIV studies and 7 from the smoke-flow visualization studies. The development of the vortex core in the direction of plasma forcing, x_c^*, is shown in figure 7(*a*) and the development of the vortex

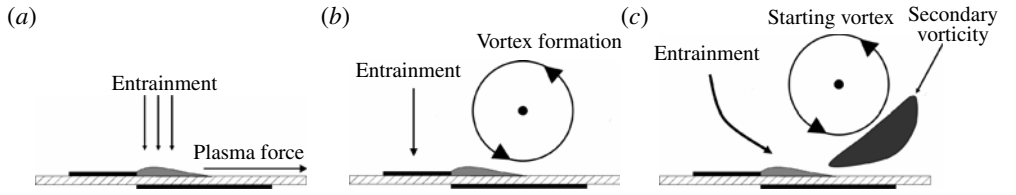

FIGURE 6. Entrainment by the plasma actuator and the development of the starting vortex: (*a*) plasma initiation, (*b*) vortex formation, and (*c*) generation of secondary vorticity.

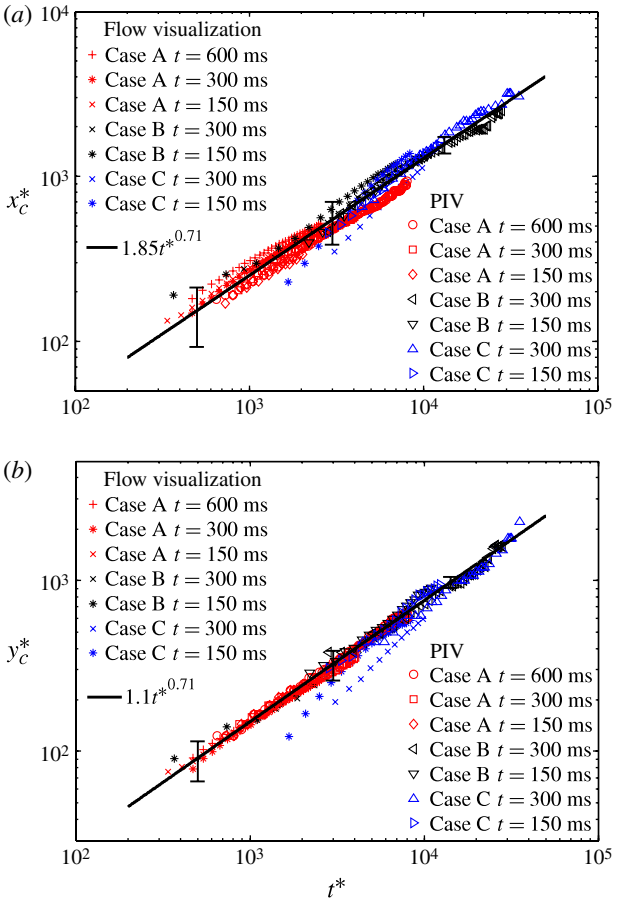

FIGURE 7. (Colour online) Vortex core scalings: (*a*) x_c^* versus t^* and (*b*) y_c^* versus t^*.

core away from the wall, y_c^*, is shown in figure 7(*b*). Error bars indicate the spread of data to two standard deviations from the mean vortex core location of the 20–25 flow visualization events. We see in figure 7 that the vortex core locations made with the PIV and the smoke-flow visualizations are in excellent agreement. Some of the data in figure 7 deviate from a straight line with an increase in time. This apparent nonlinearity in the data seems to be enhanced as the strength of plasma forcing is increased, which may be due to an increased interaction of the developing starting

vortex with the secondary vorticity on the wall. Since the vortical flow being observed is not steady, the location of the vortex core may not be tracked accurately from flow visualization using steady smoke injection. This may explain why the location of the vortex core in the x- and y-directions is underestimated as the induced velocity by DBD plasma is increased in case C. Shin & Raja (2007) also observed an increased scatter in the peak current density of the DBD as the applied frequency of the DBD plasma actuator is increased. This may have caused greater deviation in the location of the vortex core for case C.

The data across the 14 data sets collapse to a straight line when plotted in log–log axes. Therefore, the development of the vortex core should be represented by a power law of the form

$$x_c^* = \kappa_1 t^{*q}, \quad y_c^* = \kappa_2 t^{*q}. \tag{3.1}$$

Here, the exponent q is 0.71 and the coefficients κ_1 and κ_2 are 1.85 and 1.10, respectively. The starting vortex travels at 31° to the wall, which is given by $\arctan(\kappa_2/\kappa_1)$. This angle is independent of U_0, which is valid up to 1.36 m s^{-1} with the voltages and frequencies we have tested. To understand the physics behind the power law constant q, we need to study both the kinematics and the dynamics of the starting vortex. If we approximate $q = 0.71$ by a close rational number 2/3, the vortex core location, x_c and y_c, can be expressed as $x_c \sim \nu^{1/3} U_0^{1/3} t^{2/3}$ and $y_c \sim \nu^{1/3} U_0^{1/3} t^{2/3}$, respectively. Similarly, the vortex core velocity U_c of the induced plasma flow can be expressed as $U_c \sim \nu^{1/3} U_0^{1/3} t^{-1/3}$ since $U_c \sim \mathrm{d}x_c/\mathrm{d}t$. Therefore, self-similarity variables for a starting vortex can be given in the form

$$\xi \sim \frac{x}{\nu^{1/3} U_0^{1/3} t^{2/3}}, \quad \eta \sim \frac{y}{\nu^{1/3} U_0^{1/3} t^{2/3}}, \quad \tau \sim \frac{U}{\nu^{1/3} U_0^{1/3} t^{-1/3}}. \tag{3.2}$$

The similarity groups derived from the experimental power law of the trajectory show resemblance to the similarity groups derived by Cantwell (1986). Here, Cantwell investigated a general transient problem, where a non-dimensional impulse,

$$I(t) = \frac{M t^{(n-1)}}{(n-1)}, \tag{3.3}$$

was applied to create a jet. Here, M is a force–amplitude parameter with dimension $L^3 T^{-n}$. The exponent n is defined by the forcing type. For example, $n = 1$ is for an impulse, $n = 2$ for a constant force and $n = 3$ for a ramp force. He then used the Euler equations to form similarity groups, given by

$$\xi = \frac{x}{M^{1/3} t^{n/3}}, \quad \eta = \frac{y}{M^{1/3} t^{n/3}}, \quad \tau = \frac{U}{M^{1/3} t^{(n/3)-1}}. \tag{3.4}$$

Our results indicate that the plasma actuator creates momentum, which increases linearly with time: see figure 5. This suggests that the force produced is constant. Therefore, the exponent, n, in Cantwell's analysis is 2. Substitution of $n = 2$ into (3.4) predicts that the trajectory and the velocity of a starting vortex should scale with $t^{2/3}$ and $t^{-1/3}$, respectively, which is in agreement with the analysis shown in (3.2) if we take $M \sim \nu U_0$.

To evaluate the similarity laws, the velocity data for case A are plotted using the self-similarity variables in (3.2) and presented in figure 8. This figure clearly shows the validity of the similarity law over a large range of t^* during the steady state. The vortex core remains constant at $(\xi, \eta) \approx (0.70, 0.52)$. In addition, the velocity fields

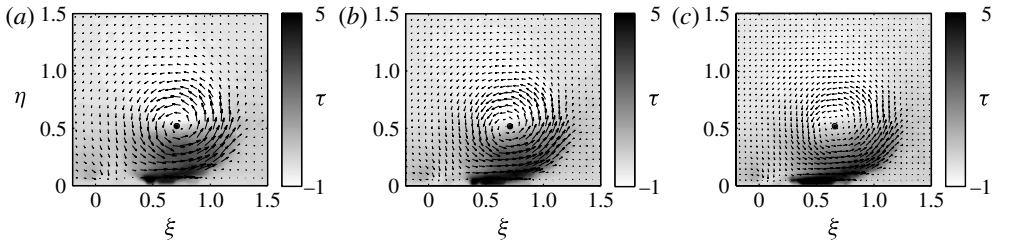

FIGURE 8. Self-similarity of the starting vortex for case A at (*a*) $t^* = 3000$, (*b*) $t^* = 4000$, and (*c*) $t^* = 5000$. A black dot in each case indicates the location of the centre of the vortex core.

show an asymmetric distribution. The positive velocity underneath the vortex core is a result of the plasma wall jet, which is developing due to the DBD plasma forcing, while the negative velocity above the core is due to the induction of the vortex and a characteristic of a vortex velocity profile.

Self-similar analysis based on our experimental results shows that $U \sim t^{-1/3}$, yet the maximum velocity U_m representing the velocity scale is nearly constant. We investigated this anomaly by examining the maximum velocity location in (ξ, η) space during the steady state. We found that the location of maximum velocity does not stay at the same location in (ξ, η) coordinates, suggesting that the self-similarity of the starting vortex does not extend to the region very close to the wall, $\eta < 0.1$.

The starting vortex has both primary and secondary vorticity, as shown in figure 3. The circulation, Γ, associated with these can be obtained by integrating the primary and secondary vorticity in each PIV image, as

$$\Gamma = \int_A \omega_z \, \mathrm{d}A. \tag{3.5}$$

Figures 9(*a*) and 9(*b*) represent the positive and negative circulation for cases A and B, respectively. Here, the plasma actuation is stopped at $t = 600$ ms ($t^* = 8100$) for case A and at $t = 300$ ms ($t^* = 28\,100$) for case B. In both cases, there are exponential start-ups in the circulation data, which is similar to the momentum data, figure 5. The circulation of the starting vortex increases with the momentum added by plasma. It is also apparent from figure 9 that the magnitude of the secondary vorticity is of the same order as the primary vorticity for the cases presented. Since $U \sim t^{-1/3}$ and $x \sim t^{2/3}$, the circulation should scale as $\Gamma \sim Ux \sim t^{1/3}$. It can be seen in figure 9(*a*) that this fits the case A data well. It should be noted, however, that some vorticity regions can move out of the control volume at large t^*, which could explain why the curve fit of $\Gamma \sim t^{1/3}$ to the data is not as good in case B for $t^* > 11\,000$.

4. Conclusions

The flow field around an asymmetric dielectric-barrier-discharge plasma actuator has been studied using particle image velocimetry and smoke-flow visualizations in quiescent air. On initiation of DBD plasma a starting vortex is created, which rolls up to form a coherent, self-similar structure. The momentum produced by the DBD plasma actuator increases linearly with time, suggesting that the DBD plasma actuator entrains and accelerates the surrounding fluid with a constant force. The velocity induced by the DBD plasma actuator was found to reach a steady state where the

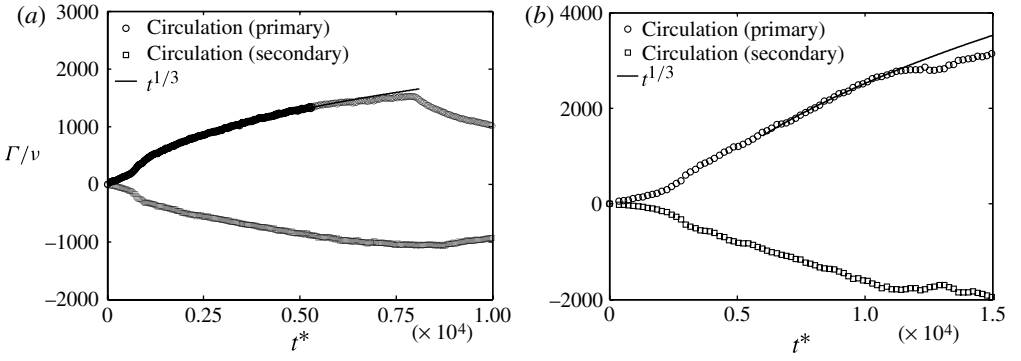

FIGURE 9. Circulation created by the starting vortex for (*a*) case A with plasma duration $t^* = 8100$ ($t = 600$ ms) and (*b*) case B with plasma duration $t^* = 28\,100$ ($t = 300$ ms).

starting vortex became self-similar. The fluid ejected laterally by the plasma actuator is replenished by the entrained flow, which leads to the generation of vorticity and circulation of the starting vortex. Secondary vorticity generated due to the no-slip boundary condition has been observed to wrap around the starting vortex and steer its trajectory away from the wall at an angle of 31°. The wall-parallel and wall-normal distances of the vortex core were observed to scale with a power law, with $t^{2/3}$, while the velocity field of the starting vortex, obtained from the similarity law, scales with $t^{-1/3}$ and the evolution of circulation with $t^{1/3}$.

Acknowledgement

This work was jointly funded by the FP6 framework programme AVERT and the Engineering and Physical Sciences Research Council.

REFERENCES

ALLEN, J. J. & CHONG, M. S. 2000 Vortex formation in front of a piston moving through a cylinder. *J. Fluid Mech.* **416**, 1–28.

ALLEN, J. J. & LOPEZ, J. M. 2007 Transition processes for junction vortex flow. *J. Fluid Mech.* **585**, 457–467.

ALLEN, J. J. & NAITOH, T. 2007 Scaling and instability of a junction vortex. *J. Fluid Mech.* **574**, 1–23.

CANTWELL, B. J. 1986 Viscous starting jets. *J. Fluid Mech.* **173**, 159–189.

CHOI, K.-S., JUKES, T. N. & WHALLEY, R. D. 2011 Turbulent boundary-layer control with plasma actuators. *Phil. Trans. R. Soc.* A **369**, 1443–1458.

CONLON, B. P. & LICHTER, S. 1995 Dipole formation in the transient planar wall jet. *Phys. Fluids* **7** (5), 999–1014.

CORKE, T. C., ENLOE, C. L. & WILKINSON, S. P. 2010 Dielectric barrier discharge plasma actuators for flow control. *Annu. Rev. Fluid Mech.* **42**, 505–529.

ENLOE, C. L., MCHARG, M. G. & MCLAUGHLIN, T. E. 2008 Time-correlated force production measurements of the dielectric barrier discharge plasma aerodynamic actuator. *J. Appl. Phys.* **103**, 073302.

ENLOE, C. L., MCLAUGHLIN, T. E., VANDYKEN, R. D., KACHNER, K. D., JUMPER, E. J., CORKE, T. C., POST, M. & HADDED, O. 2004 Mechanisms and responses of a single dielectric barrier plasma actuator: geometric effects. *AIAA J.* **42** (3), 595–604.

GHERARDI, N., GAMAL, G., GAT, E., RICARD, A. & MASSINES, F. 2000 Transition from glow silent discharge to micro-discharges in nitrogen gas. *Plasma Sources Sci. Technol.* **9**, 340–346.

JUKES, T. N. & CHOI, K.-S. 2009 Control of unsteady flow separation over a circular cylinder using dielectric-barrier-discharge surface plasma. *Phys. Fluids* **21**, 094106.

JUKES, T. N., CHOI, K.-S., JOHNSON, G. A. & SCOTT, S. J. 2006 Characterisation of surface plasma-induced wall flows through velocity and temperature measurement. *AIAA J.* **44**, 764–771.

KOTSONIS, M., GHAEMI, S., VELDHUIS, L. & SCARANO, F. 2011 Measurement of the body force field of plasma actuators. *J. Appl. Phys.* D **44**, 045204.

KRIEGSEIS, J., GRUNDMANN, S. & TROPEA, C. 2011 Power consumption, discharge capacitance and light emission as measures for thrust production of dielectric barrier discharge plasma actuators. *J. Appl. Phys.* **110**, 0133051.

MOREAU, E. 2007 Airflow control by non-thermal plasma actuators. *J. Phys.* D **40** (3), 605–636.

ROBINSON, M 1962 A history of the electric wind. *Am. J. Phys.* **30** (5), 366–372.

SHIN, J. & RAJA, L. L. 2007 Run-to-run variations, asymmetric pulses, and long time-scale transient phenomena in dielectric-barrier atmospheric pressure glow discharges. *J. Phys.* D **40**, 3145–3154.

WESTERWEEL, J 1997 Fundamentals of digital particle image velocimetry. *Meas. Sci. Technol.* **8**, 1379–1392.

WHALLEY, R. D. 2011 Turbulent boundary-layer control with DBD plasma actuators using spanwise travelling-wave technique. PhD thesis, University of Nottingham.

WHALLEY, R & CHOI, K.-S. 2010 Starting, traveling and colliding vortices: Dielectric-barrier-discharge plasma in quiescent air. *Phys. Fluids* **22**, 091105.